Distance Distributions and Anisotropy Decays of Troponin C and Its Complex with Troponin I†

Herbert C. Cheung,*,‡ Chien-Kao Wang,‡,§ Ignacy Gryczynski,∥ Wieslaw Wiczk,∥ Gabor Laczko,∥ Michael L. Johnson,⊥ and Joseph R. Lakowicz∥

Department of Biochemistry, University of Alabama at Birmingham, UAB Station, Birmingham, Alabama 35294, Department of Biological Chemistry, University of Maryland at Baltimore School of Medicine, 660 West Redwood Street, Baltimore, Maryland 21201, and Department of Pharmacology, University of Virginia, Charlottesville, Virginia 22098

Received November 2, 1990; Revised Manuscript Received February 4, 1991

ABSTRACT: We used frequency domain measurements of fluorescence resonance energy transfer to recover the distribution of distances between Met 25 and Cys 98 in rabbit skeletal troponin C. These residues were labeled with dansylaziridine as energy donor and 5-(iodoacetamido)eosin as acceptor and are located on the N- and C-terminal lobes of the two-domain protein, respectively. We developed a procedure to correct for the fraction of the sample that was incompletely labeled with the acceptor independent of chemical data. At pH 7.5 and in the presence of Mg^{2+}, the mean distance was near 15 Å with a half-width of the distribution of 15 Å; when Mg^{2+} was replaced by Ca^{2+}, the mean distance increased to 22 Å with a decrease in the half-width by 4 Å. Similar but less pronounced differences in the mean distance and half-width between samples containing Mg^{2+} and Ca^{2+} were also observed with troponin C complexed to troponin I. The results suggest that the conformation of troponin C is altered by Ca^{2+} binding to the Ca^{2+}-specific sites and displacing bound Mg^{2+} at the Ca^{2+}/Mg^{2+} sites. This alteration may play an important role in Ca^{2+} signaling in muscle. At pH 7.5, the anisotropy decays of the donor-labeled troponin C showed two components, with the long rotational correlation time (12 ns) reflecting the overall motion of the protein. When the pH was lowered from 7.5 to 5.2, the mean distribution distance of apotroponin C increased from 22 to 32 Å and the half-width decreased by a factor of 2 from 13 to 7 Å. The long correlation time of apotroponin C increased to 19 ns at the acidic pH. These results are discussed in terms of a model in which skeletal troponin C is a dimer at low pH and enable comparison of the solution conformation of the protein at neutral pH with a crystal structure obtained at pH 5.2. While the conformation of the monomeric unit of troponin C dimer at pH 5.2 is extended and consistent with the crystal structure, the conformation at neutral pH is likely more compact than the crystal structure predicts.

Signal transmission is a major process by which many biological systems are activated. In muscle the signal is cytosolic calcium. Its elevation in myoplasm from submicromolar to micromolar concentrations is obligatory for activation of actomyosin ATPase and initiation of the contraction–relaxation cycle. Troponin C is one of the three subunits of troponin (molecular weight 78 000) and the Ca^{2+}-binding protein directly involved in the transmission of the Ca^{2+} signal in skeletal and cardiac muscle. TnC[1] from mammalian and avian skeletal muscle has four sites for Ca^{2+}. Two sites (sites I and II) are located in the N-terminal half of the single polypeptide chain (molecular weight 18 000) and bind Ca^{2+} specifically with a low affinity ($K_a \approx 10^5$ M^{-1}) for Ca^{2+}. The other two sites (sites III and IV), which are located in the C-terminal half, bind both Ca^{2+} with a high affinity ($K_a \approx 10^7$ M^{-1}) and Mg^{2+} competitively. Troponin and tropomyosin form a tight complex, both in vivo and in vitro, and this complex is bound to the actin filament. It is currently thought that Ca^{2+} binding to TnC induces structural changes in the protein and these changes are transmitted to the other troponin subunits. The transmission leads to alteration of the binding between TnI and actin and between actin and myosin, thereby allowing actin to interact with myosin and activating actomyosin ATPase. The initial Ca^{2+} binding has been viewed as the triggering step in a cascade of structural changes that are propagated across the thin filament. Ultimately, the mechanism of signal transmission must be elucidated on the basis of the structural changes of the proteins that make up the entire assembly. To fully appreciate these changes, we require an understanding of the energetics of protein assembly and the conformational dynamics of individual proteins and proteins complexes.

The initial crystal structures of turkey (Herzberg & James, 1985) and chicken (Sundaralingam et al., 1985a) skeletal TnC have been refined at 2.2 Å (Herzberg et al., 1986) and 2.0 Å (Satyshur et al., 1988) resolution, respectively. X-ray diffraction results show that TnC has an unusual dumbbell

†This work was supported by Grants AR 25193 and AR 31239 (H.C.C.) and GM 35154 (J.R.L.) from the National Institutes of Health and DMB 8804931 from the National Science Foundation (J.R.L.). J.R.L., G.L., and W.W. acknowledge support from the Medical Biotechnology Center at the University of Maryland. Instrumentation at the University of Maryland was provided by grants from the National Science Foundation (DMB 8511065) and the Center for Fluorescence Spectroscopy (NSF DIR 8710401).

‡University of Alabama at Birmingham.

§Present address: Department of Physiology and Biophysics, University of Washingtom, Seattle, WA.

∥University of Maryland at Baltimore.

⊥University of Virginia.

[1] Abbreviations: TnC, troponin C; TnI, troponin I; DNZ, dansylaziridine; IAEDANS, *N*-(iodoacetyl)-*N'*-(1-sulfo-5-naphthyl)ethylenediamine; IAE, 5-(iodoacetamido)eosin; TnC–DNZ, troponin C labeled with DNZ as energy donor; TnC–DNZ–IAE, troponin C labeled with DNZ as energy donor and IAE as energy acceptor; DTT, dithiothreitol; EGTA, ethylene glycol bis(β-aminoethyl ether)-*N,N,N',N'*-tetraacetic acid; FRET, fluorescence resonance energy transfer; D, energy donor; A, energy acceptor; D–A, donor–acceptor; GuHCl, guanidine hydrochloride; hw, half-width (full width of the Gaussian at the half-maximum height).

0006-2960/91/0430-5238$02.50/0

shape of about 75 Å long with the N- and C-terminal regions folded into two globular domains (diameter about 25 Å). The two domains are linked by a 32-residue 9-turn α-helix (residues 75–106). The structures of both proteins are very similar, and their crystals contain bound Ca^{2+} at sites III and IV. The two Ca^{2+}-specific sites (sites I and II) are devoid of bound metals in the crystal. The middle one-third of the long central helix (D/E helix) is exposed to solvent and not in contact with neighboring molecules, whereas the helical segments at both ends of the helix are either partially or completely buried in the globular domains. The central helix is believed to be stabilized by salt bridges (Sundaralingam et al., 1985b) between oppositely charged side chains 3 or 4 residues apart and water bridges. It has been suggested that these interactions may also be important in the nucleation of the helix (Satyshur et al., 1988).

Since TnC crystals were obtained at pH 5.0–5.2 for crystallographic studies, the question has been raised as to whether the conformation of TnC in neutral solution is comparable to that at acidic pH and in what way an extended helical conformation may be related to Ca^{2+} signaling in muscle. Cheung and Wang (1985) showed in a preliminary study that the fluorescence resonance energy transfer distance between Met 25 and Cys 98 was pH dependent, decreasing by a factor of 2 from pH 7.5 to 5.2. This result raised the possibility that the protein may have a compact conformation in neutral solution and become elongated only in an acidic medium. In the present work we have extended the previous study by using frequency domain methods recently developed in these laboratories (Lakowicz & Maliwal, 1985; Lakowicz et al., 1986) to analyze the FRET data in terms of the distribution of donor–acceptor distances (Haas et al., 1975; Amir & Haas, 1987; Lakowicz et al., 1987, 1988). Specifically, we measured the intensity decays of a donor linked to Met 25, in the absence and presence of an acceptor attached to Cys 98. These decays were analyzed in terms of a distribution of donor-to-acceptor distances with use of the frequency response of the singly donor-labeled protein as the control (Lakowicz et al., 1987, 1988). The presence of an acceptor in close proximity results in a decrease of donor decay time due to nonradiative energy transfer to the acceptor. Additionally, if the acceptor is present at a range of distances then there is a range of transfer rates, which appears as increased heterogeneity in the donor decay. We recovered the distributions of D–A distances by using a comparative analysis of the donor decay and the decay of the donor–acceptor pair. Our previous studies have shown that this method can provide useful information on the distribution of distances between two sites in a protein, as reflected in both the average D–A distance and width of the recovered distribution. Using this method, we examined the effects of pH, metal ions, and complexation with troponin I on the distance between Met 25 and Cys 98 in troponin C and deduced from these results the possible role of protein dynamics in calcium activation of muscle.

Theory

Distance Distribution Analysis

The theory for frequency domain measurements of energy transfer to recover distance distributions has been described previously in detail (Lakowicz et al., 1988). We summarize the procedures used for the present analysis. The Forster distance R_0 for energy transfer (Forster, 1948) is calculated in the usual manner from the spectral properties of the donor and acceptor. In our case, the intensity decay of the donor is not single-exponential, even in the absence of energy transfer to an acceptor. Hence, we first analyze the decay of the donor alone using the multiexponential model

$$I_D(t) = \sum_i \alpha_{Di} \exp(-t/\tau_{Di}) \tag{1}$$

where α_{Di} values are the preexponential factors and τ_{Di} values are the associated decay times for the donor in the absence of acceptor. The purpose of this analysis is to obtain a parameterized form for the donor decay, for subsequent use in the distance distribution analysis. We assume that the Forster distances (R_0) for transfer from each component in the donor decay are the same, and the transfer rates are given by

$$k_{DAi} = \frac{1}{\tau_{Di}}\left(\frac{R_0}{r}\right)^6 \tag{2}$$

In eq 2 we assumed that the transfer rates were proportional to the inverse decay times, which is known to be valid for single-exponential donor decays. The distance-dependent donor decay times are then given by

$$\frac{1}{\tau_{DAi}} = \frac{1}{\tau_{Di}} + \frac{1}{\tau_{Di}}\left(\frac{R_0}{r}\right)^6 \tag{3}$$

With this assumption, the intensity decay of a D–A pair spaced by a unique distance r is given by

$$I_{DA}(r,t) = \sum_i \alpha_{Di} \exp\left[-\frac{t}{\tau_{Di}} - \frac{t}{\tau_{Di}}\left(\frac{R_0}{r}\right)^6\right] \tag{4}$$

and the observed decay for an ensemble of D–A pairs is given by

$$I_{DA}(t) = \int_0^\infty P(r)\, I_{DA}(r,t)\, dr \tag{5}$$

where $P(r)$ is the probability distribution of distances. In practice, the integral in eq 5 is calculated over a range of distances from r(min) to r(max), where the lower limit is about 5 Å and the upper limit is about 100 Å. The results of the analysis are usually not dependent upon the precise values of the limits. In the present report, we assume the distance probability distribution is a Gaussian function

$$P(r) = \frac{1}{Z}\frac{1}{\sigma\sqrt{2\pi}} \exp\left[-\frac{1}{2}\left(\frac{r-\bar{r}}{\sigma}\right)^2\right] \tag{6a}$$

where $\bar{r}$ is the average distance and σ the standard deviation of the distribution, which is related to the half-width (hw) by hw = 2.354σ. Since the distance integration limits do not range from $-\infty$ to $+\infty$, the area under $P(r)$ is not necessarily unity. Hence, $P(r)$ is normalized by the area, and the normalization factor Z is given by

$$Z = \int_{r(\min)}^{r(\max)} \frac{1}{\sigma\sqrt{2\pi}} \exp\left[-\frac{1}{2}\left(\frac{r-\bar{r}}{\sigma}\right)^2\right] dr \tag{6b}$$

Irrespective of the form of the decay, the phase (ϕ_ω) and modulation (m_ω) data, at any frequency ω, can be calculated from the sine and cosine transforms

$$N_\omega = \frac{\int_0^\infty I(t) \sin(\omega t)\, dt}{\int_0^\infty I(t)\, dt} \tag{7}$$

$$D_\omega = \frac{\int_0^\infty I(t) \cos(\omega t)\, dt}{\int_0^\infty I(t)\, dt} \tag{8}$$

For the multiexponential decay law these transforms can be represented analytically (Lakowicz et al., 1984). These transforms for the multiexponential donor alone are given by

$$N_\omega^D = \frac{1}{J^D}\sum_i \frac{\omega\alpha_{Di}\tau_{Di}^2}{1+\omega^2\tau_{Di}^2} \quad (9)$$

$$D_\omega^D = \frac{1}{J^D}\sum_i \frac{\alpha_{Di}\tau_{Di}}{1+\omega^2\tau_{Di}^2} \quad (10)$$

$$J^D = \sum_i \alpha_{Di}\tau_{Di} \quad (11)$$

If there is a distribution of distances, the transforms are calculated numerically from

$$N_\omega^{DA} = \frac{1}{J^{DA}}\int_0^\infty \sum_i \frac{P(r)\,\omega\alpha_{Di}\tau_{DAi}^2}{1+\omega^2\tau_{DAi}^2}\,dr \quad (12)$$

$$D_\omega^{DA} = \frac{1}{J^{DA}}\int_0^\infty \sum_i \frac{P(r)\,\alpha_{Di}\tau_{DAi}}{1+\omega^2\tau_{DAi}^2}\,dr \quad (13)$$

where the superscript and subscript DA refers to a donor–acceptor pair and the normalization factor J^{DA} is given by

$$J^{DA} = \int_0^\infty I_{DA}(t)\,dt \quad (14)$$

It is important to note that a multiexponential decay for the donor does not introduce any additional parameters into the analysis because the intrinsic decays of the donor are measured in a separate experiment, using a sample without acceptor. The decay data from the donor are fitted by use of the multiexponential model, with the parameters (α_{Di} and τ_{Di}) in eqs 12 and 13 being held constant during the least-squares analysis.

The parameters describing the intensity decay (α_{Di} and τ_{Di}) are found by use of a nonlinear least-squares procedure (Bevington, 1969; Lakowicz et al., 1984; Gratton et al., 1984). The calculated (c) phase and modulation values for the assumed decay law are given by

$$\phi_{c\omega} = \arctan\left(\frac{N_\omega}{D_\omega}\right) \quad (15)$$

$$m_{c\omega} = (N_\omega^2 + D_\omega^2)^{1/2} \quad (16)$$

The parameter values are estimated by minimizing χ_R^2

$$\chi_R^2 = \frac{1}{\nu}\sum_\omega\left(\frac{\phi_\omega - \phi_{c\omega}}{\delta\phi}\right)^2 + \frac{1}{\nu}\sum_\omega\left(\frac{m_\omega - m_{c\omega}}{\delta m}\right)^2 \quad (17)$$

where ν is the number of degrees of freedom and $\delta\phi = 0.2°$ and $\delta m = 0.005$ are the experimental uncertainties in the measured phase and modulation values.

At present there is no analytical method to calculate the uncertainties in the derived parameters from the experimental data. Our analysis program calculates the uncertainties by examination of the range of parameter values that are consistent with the data (Johnson, 1983). We also examined the dependence of χ_R^2 surfaces for fixed values of the parameters following adjustment of the other values to minimize χ_R^2. Both these methods should account for correlation between the parameters, which allows the parameter values to vary in a concerted manner without significantly altering χ_R^2.

Correction for Incomplete Labeling by Acceptor

For measurements of distance distributions, it is essential to obtain complete labeling with acceptor or to correct for the amount of protein not labeled with acceptor. Incomplete labeling with the donor is not a problem because these protein molecules do not contribute to the donor decay. On the other hand, donor-labeled proteins containing no acceptor cannot participate in energy transfer and their emission will be unquenched. Consequently, these molecules will contribute to the observed fluorescence in excess of the other molecules participating in energy transfer. A correction must be made for this nonstoichiometric labeling (underlabeling) of the protein by acceptor. The correction can be readily made if chemical data of the extent of acceptor labeling are available. Alternatively, the correction can be estimated from the measured fluorescence intensity decay data. In this procedure, we assume that the observed intensity $I_{obs}(t)$ is the result of that due to donor alone [$I_D(t)$] and that due to the D–A pairs [$I_{DA}(t)$]. Hence, the observed intensity decay is given by

$$I_{obs}(t) = (1 - L)\,I_D(t) + L\,I_{DA}(t) \quad (18)$$

$$I_{obs}(t) = (1 - L)\sum_i \alpha_{Di}\exp(-t/\tau_{Di}) + L\int_0^\infty P(r)\sum_i \alpha_{Di}\exp[-t/\tau_{Di} - (-t/\tau_{Di})(R_o/r)^6]\,dr \quad (19)$$

where L is the fractional labeling with acceptor. One notices in eqs 18 and 19 that the donor alone molecules contribute in excess of their molar proportion due to higher relative intensity of $I_D(t)$ vs $I_{DA}(t)$. The frequency response for this case of partial labeling by acceptor can be calculated from

$$N_\omega^{obs} = \frac{(1-L)J^D N_\omega^D + LJ^{DA}N_\omega^D}{(1-L)J^D + LJ^{DA}} \quad (20)$$

$$D_\omega^{obs} = \frac{(1-L)J^D D_\omega^D + LJ^{DA}D_\omega^{DA}}{(1-L)J^D + LJ^{DA}} \quad (21)$$

A complete description of this procedure will be published elsewhere (Lakowicz et al., 1991a). In our procedure, the extent of labeling (L) can be determined by varying L to yield the minimum value of χ_R^2. Once this was done for a given preparation, L was held constant in all subsequent analyses.

Anisotropy Decay

Anisotropy decays were obtained from the frequency response of the polarized emission as described previously in detail (Lakowicz et al., 1985; Miliwal & Lakowicz, 1986). The data were fitted to a double-exponential anisotropy decay law

$$r(t) = \sum_i r_i \exp(-t/\theta_i) \quad (22)$$

where r_i are the amplitudes of the components associated with the correlation times θ_i. The total anisotropy $r_0 = r_1 + r_2$ was considered to be a variable parameter.

Materials and Methods

TnC and TnI were isolated from rabbit skeletal muscle as described previously. Troponin was obtained as in our previous work (Cheung et al., 1982), and TnC was separated from isolated troponin as described by Perry and Cole (1974). Troponin B (TnI·TnC complex) was isolated (Wilkinson, 1974) and used as the starting material for preparation of TnI. The isolated subunits were shown to be homogeneous with use of dodecyl sulfate–polyacrylamide gel electrophoresis. Protein concentrations were determined by use of $E(1\%) = 3.97$ at 280 nm for TnI (Perry, 1974) and 1.75 at 276 nm for TnC (McCubbin et al., 1982). The molecular weights of TnI and TnC were taken as 21 000 and 18 000, respectively. The extent

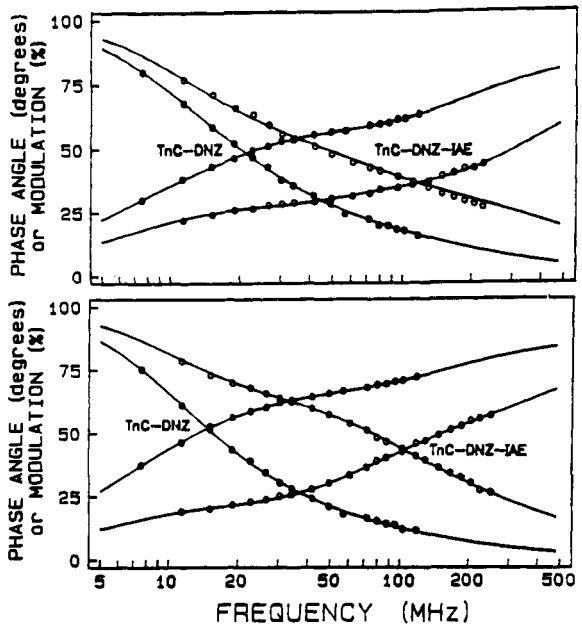

FIGURE 1: Frequency domain phase and modulation data for donor-labeled TnC (TnC-DNZ, ●) and donor-acceptor-labeled TnC (TnC-DNZ-IAE, ○): top, pH 7.5; bottom, pH 5.2. The phase angle increases and the modulation decreases with increasing frequency.

of labeling of TnC with DNZ was found to be 99% and with IAE 92% from absorbance data with use of a molar extinction coefficient of 3.98×10^3 M^{-1} cm^{-1} at 350 nm for DNZ and 8.3×10^4 M^{-1} cm^{-1} at 528 nm for IAE. Whenever necessary, the absorbance of TnC at 276 nm was corrected for probe absorption in order to estimate protein concentration as described previously (Wang & Cheung, 1986).

All experiments were performed at 20 °C and pH 7.5 (50 mM Tris) or pH 5.2 (50 mM MES). The buffers also contained 0.3 M KCl, 1 mM EGTA, and 0.5 mM DTT. To examine the effects of divalent cations, these ions were added as the chloride salts to 1.3 mM for Ca^{2+} and 10 mM for Mg^{2+}.

Frequency domain fluorescence data were obtained on the instrument described previously (Lakowicz et al., 1986). The excitation source was a 3.79-MHz train of pulses, about 5 ps wide, obtained from the cavity-dumped output of a synchronously pumped pyridine 2 dye laser. The dye laser output was frequency-doubled to 355 nm. This source was intrinsically modulated to a range of GHz and used directly to excite the sample. The modulated emission was detected by a microchannel plate photomultiplier tube, R1564U (Hamamatsu Corp.), which was externally cross-correlated. All intensity decays were measured with use of rotation-free polarized conditions, with the donor emission selected by a 480-nm interference filter, 10-nm bandwidth.

Results

Emission Spectra of Donor- and Donor-Acceptor-Labeled TnC

The quantum yield of the donor dansylaziridine decreased by 27% in the presence of Mg^{2+} and increased by a factor of 2.1 in the presence of Ca^{2+}, with corresponding spectral shifts of 5 nm to the red and 12 nm to the blue, respectively. When complexed to TnI, the dansyl quantum yield increased by a factor of 1.79 with a 12-nm blue shift of the spectral peak. The emission of the acceptor IAE in singly labeled TnC showed a maximum at 556 nm and its emission was negligible at wavelengths below 500 nm (Wang & Cheung, 1986). These spectral properties enabled us to isolate the donor emission from the D–A-labeled TnC with a 480-nm interference filter.

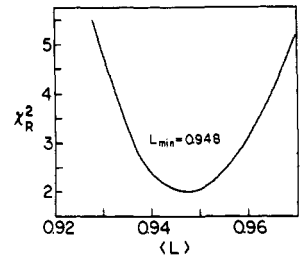

FIGURE 2: Dependence of χ_R^2 on the extent of acceptor labeling, $\langle L \rangle$, assumed in the least-squares analysis. The hw and $\bar{r}$ were both variable parameters as L was varied. The angular brackets indicate the extent of labeling (L) being held constant at the indicated values.

Figure S1 [supplementary material (see paragraph at end of paper regarding supplementary material)] shows that the emission of the acceptor is adequately rejected by the interference filter.

Donor Decays as the Extent of Labeling with Acceptor

Representative frequency responses of the D- and D–A-labeled TnC are shown in Figure 1. In each case, the data for the D–A pairs are shifted to higher frequencies, which is the result of the shorter donor decay times in the presence of energy transfer. The unusual shape of the frequency responses indicates that the decays are strongly heterogeneous in the absence or presence of acceptor. This is illustrated by the multiexponential analysis summarized in Table SI in the supplementary material. In each case it was not possible to fit the data with use of a single decay time, the χ_R^2 values ranging from 1000 to 8000. The multiple-decay characteristic of TnC-DNZ is indicated by a χ_R^2 value of 2000 for a one-exponential fit. The fits with three decay times are characterized by a much improved and acceptable χ_R^2 value of 1.2. In spite of the strong heterogeneity displayed by the TnC-DNZ, it is still possible to detect additional heterogeneity due to the presence of the acceptor. The χ_R^2 for apo-TnC-DNZ-IAE is increased to 4527 for the one-exponential fit and improved to 4.8 for a fit with three decay times. In each of the other cases, the presence of acceptor results in a further increase in χ_R^2 for the one- and two-exponential fits. This increased complexity in the frequency response is due to both the distribution of D–A and incomplete labeling with acceptor.

To determine the fractional extent of labeling of TnC with the acceptor, we examined how χ_R^2 was dependent upon the fractional labeling (L). In this procedure we used the α_{Di} and τ_{Di} values from the donor alone analysis (Table SI). The parameters describing the distribution ($\bar{r}$ and hw) were allowed to vary to obtain the minimum value of χ_R^2. This procedure yielded an extent of labeling near 95% as shown in Figure 2, which is in good agreement with the value of 92% determined from the absorbance measurement. Equivalent values of L were obtained by allowing L to be a variable parameter during the distance distribution fits. The extent of labeling with acceptor (L = 0.948) was held constant in the subsequent analyses.

Analysis of Distance Distribution in TnC

The frequency domain intensity decays determined under a variety of experimental conditions were used to recover the distance distributions. Representative distribution fits are shown in Figure 3. It is seen that the frequency responses for donor–acceptor-labeled TnC are well fitted by the distance distribution model. These results are summarized in Table I. The fractional intensity of the DA pairs (f_{DA}) was calculated on the basis of a degree of acceptor labeling (L) of 0.948 (Figure 2). This value of L is about 97% for the measured

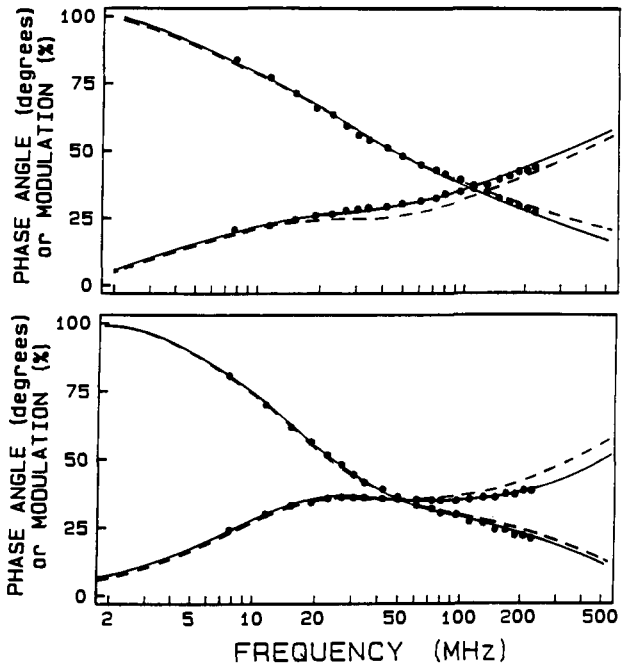

FIGURE 3: Distance distribution fits of the frequency response of donor-plus-acceptor-labeled TnC in the absence (top) and presence (bottom) of Ca^{2+} at pH 7.5. The solid lines are the best fitted curves with three decay times and a Guassian distribution. Top: $\bar{r}$ = 22.4 Å and hw = 13.3 Å; bottom: $\bar{r}$ = 22.1 Å and hw = 10.9 Å. The dashed curves were obtained by holding the half-width (hw) constant at 7 Å (top) and 15.1 Å (bottom).

Table I: Distance Distribution Analysis of Donor–Acceptor-Labeled TnC[a]

conditions	R_0 (Å)	f_{DA}[b]	E_T[c]	$\bar{r}$ (Å)	hw (Å)	χ_R^2
pH 7.5 (EGTA)	43.6	0.39	0.96	22.4	13.3	2.1
					⟨15.0⟩[d]	19.1
					⟨7.0⟩	265.1
pH 5.2 (EGTA)	48.6	0.59	0.92	31.8	7.0	2.3
				29.8	⟨13.3⟩	136.0
pH 7.5 (Mg^{2+})	41.4	0.18	0.99	15.2	15.0	1.5
					⟨17.2⟩	90.4
pH 7.5 (Ca^{2+})	48.9	0.21	0.98	22.1	10.9	4.5
					⟨15.1⟩	73.2
pH 7.5 (GuHCl)	39.6	0.69	0.88	18.0	34.7	2.6

[a] TnC was labeled with DNZ as energy donor and IAE as energy acceptor. The extent of acceptor labeling was held at 94.8% during least-squares analysis. [b] The fractional intensity of the DA pair (f_{DA}) was obtained from

$$f_{DA} = \frac{\int_0^\infty L\, I_{DA}(t)\, dt}{\int_0^\infty I_{obs}(t)\, dt}$$

[c] The transfer efficiency (E_T) was calculated from

$$E_T = 1 - \int_0^\infty I_{DA}(t)\, dt = 1 - J^{DA}$$

[d] The brackets indicate that this parameter was held fixed at the indicated value during the least-squares analysis.

extent of labeling, and the difference is within experimental uncertainty of the measured value. A small variation in L has a negligible effect in the calculated parameter. We note that the fractional intensity is higher than that for a unique D–A distance and the same degree of acceptor labeling. The transfer efficiency (E_T) is quite high in all cases. For a D–A pair that can be characterized by a single unique distance, the calculated transfer efficiencies would correspond to D–A separations considerably smaller than R_0. The inverse sixth power relationship is modified by the distribution of distances

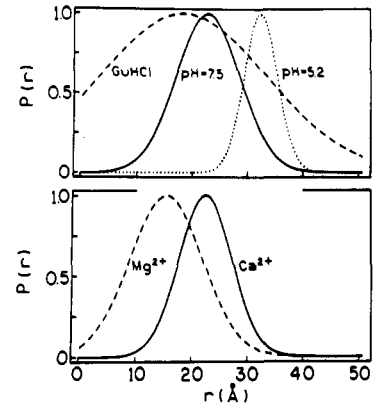

FIGURE 4: Distance distributions for TnC–DNZ–IAE in the absence of cations (top) and in the presence of Mg^{2+} and Ca^{2+} (pH 7.5, bottom). The pH for guanidine hydrochloride (GuHCl) was 7.5.

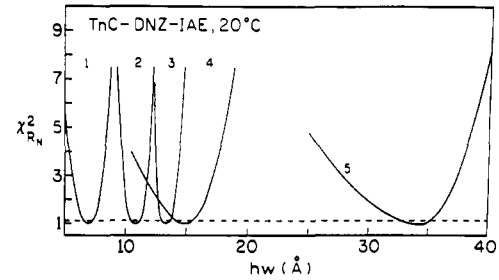

FIGURE 5: Dependence of χ_R^2 on the hw for TnC–DNZ–IAE recovered under various conditions: (1) EGTA at pH 5.2, (2) Ca^{2+} at pH 7.5, (3) EGTA at pH 7.5, (4) Mg^{2+} at pH 7.5, and (5) 6 M guanidine hydrochloride. The value of hw was held constant at the value indicated on the horizontal axis, and $\bar{r}$ was varied to minimize χ_R^2. The values of the χ_R^2 are normalized to the minimum value. The dashed line indicates the largest value of χ_R^2 with random noise in 67% of repetitive measurements.

in the present case, and the mean distances ($\bar{r}$) recovered from $P(r)$ are related to R_0 in a different way. Relatively wide distributions with half-widths ranging from 7 to 17 Å were observed. The best-fitted mean distance is 22.4 Å for apo-TnC at pH 7.5 (sample 1) and the half-width is 13.3 Å with a χ_R^2 value of 2.1. When the same data were fitted by holding the hw constant at 15 Å, the χ_R^2 value increased 8-fold to 19.4, indicating that the uncertainty in the best-fitted value was not likely more than 1–2 Å. The most striking result is the distribution recovered for apo-TnC at pH 5.2: while the mean distance is increased to 31.8 Å, the half-width is decreased by a factor of 2 to 7.0 Å. We refitted the pH 7.5 data by using the half-width (7 Å) recovered for the pH 5.2 data (Figure 3, top) and obtained a 120-fold increase in the χ_R^2 value. Conversely, we refitted the pH 5.2 data using a fixed half-width of 13.3 Å (from the pH 7.2 data) and obtained a 60-fold elevation of χ_R^2 to 136. These results indicate that the data are easily adequate to demonstrate significantly different mean distances and half-widths for TnC at the two different pH values. The effect of Mg^{2+} at pH 7.5 is a small broadening (hw = 15.0 Å) of the distribution with a substantial decrease in the average distance, and the effect of Ca^{2+} is a small decrease of the hw to 10.9 Å with no change in the mean distance. Refitting the pH 7.5 Ca^{2+} data by holding the hw constant at 15.1 Å (Figure 3, bottom) increases the χ_R^2 value by a factor of 60. These and other distributions are displayed graphically in Figure 4. When the protein is unfolded by GuHCl, the distribution is considerably broadened and the mean distance is slightly decreased.

The half-widths recovered for four of the five samples listed in Table I are within the range 7–15 Å. To further evaluate

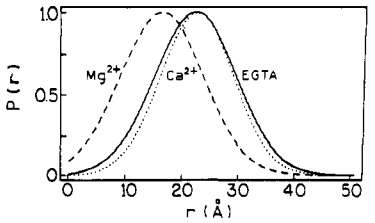

FIGURE 6: Effects of cations on the distance distribution for TnC-DNZ-IAE complexed with TnI at pH 7.5.

Table II: Distance Distribution Parameters of Donor-Acceptor-Labeled TnC Complexed to TnI (TnI·TnC)[a]

condition	R_0 (Å)	f_{DA}[b]	E_T[b]	$\bar{r}$ (Å)	hw (Å)	χ_R^2
EGTA	46.1	0.36	0.97	21.9	16.9	2.8
					(13.3)[c]	73.3
Mg^{2+}	43.8	0.30	0.98	16.1	17.2	3.1
Ca^{2+}	47.8	0.26	0.98	22.2	15.1	3.1

[a] All samples were at pH 7.5. [b] See Table I for these parameters. [c] The brackets indicate that this parameter was held fixed at the indicated value during the least-square analysis.

whether these data do indicate differences among the samples, we examined the uncertainties in the hw by calculating the χ_R^2 surfaces shown in Figure 5. These surfaces were calculated by holding the hw constant at the values indicated on the horizontal axis and allowing the mean distance $\bar{r}$ to vary until the minimum value of χ_R^2 was obtained. The range of $\bar{r}$ and hw values that are consistent with the data is approximately given by the range of values for which χ_R^2 is increased to an extent possible 67% of the time due to random error. By this criterion, it is clear that the distributions of apo-TnC at the two pH values are distinct from each other. At pH 7.5, the surfaces for TnC studied in the presence of EGTA and in Ca^{2+} do not overlap with any reasonable value for χ_R^2, which indicates that the D-A distance distributions under the two ionic conditions are different from each other. The surface for TnC at pH 7.5 in the presence of Mg^{2+} is relatively shallow, showing overlap with two other surfaces at the same pH. It intersects the surface for the EGTA sample at a low value of χ_R^2 near the 67% line. Thus, we conclude that the half-widths of the distributions of D-A distances for native TnC are different under the three ionic conditions at pH 7.5. Finally, the χ_R^2 surface for denatured TnC is distinct from all other surfaces and the distance distribution for the denatured state is different from the native state.

Distance Distribution of TnC Complexed to TnI

The distributions of D-A distances of TnC in the binary TnI·TnC complex were recovered as for isolated TnC. Table II summarizes the distribution parameters and Figure 6 shows the recovered distributions. Complexation with TnI results in a small increase in the hw of the distribution with little effect on the mean D-A distance. The half-width (16.9 Å) in the presence of TnI appears to be significantly different from that in the absence of TnI (13.3 Å), as can be seen from the elevated value of χ_R^2 when the TnI·TnC data are force fitted (Table II). Addition of Mg^{2+} to the binary complex decreases $\bar{r}$ by 6 Å without affecting the hw. When Mg^{2+} is replaced by Ca^{2+}, the mean distance increases by 6 Å and the half-width by about 2 Å. Qualitatively, these changes parallel those observed with isolated TnC.

Anisotropy Decays

A set of typical anisotropy decay data obtained at pH 7.5 and 5.2 for TnC-DNZ are shown in Figure 7. At both pH values, the decay is biexponential with a short correlation time

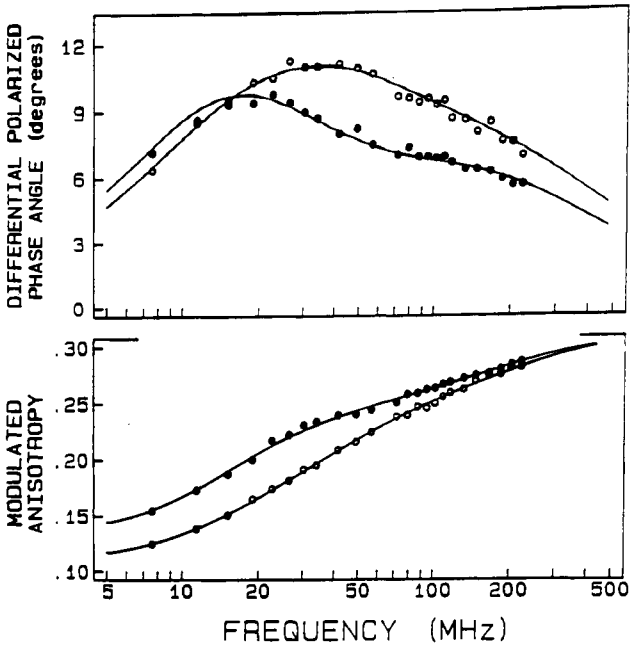

FIGURE 7: Frequency domain anisotropy data for donor-labeled TnC (TnC-DNZ) at pH 7.5 (○) and pH 5.2 (●).

Table III: Anisotropy Decays of TnC-DNZ[a]

condition	θ_i (ns)	r_{0i}	χ_R^2 1	χ_R^2 2
TnC, pH 7.5 (EGTA)	1.53	0.141	98.6	2.3
	12.46	0.171		
TnC, pH 7.5 (Mg^{2+})	1.16	0.155	140.4	2.7
	13.39	0.154		
TnC, pH 7.5 (Ca^{2+})	1.45	0.101	86.4	2.6
	12.62	0.196		
TnC, pH 5.2 (EGTA)	1.13	0.078	118.7	3.1
	19.21	0.232		
TnI·TnC, pH 7.5 (EGTA)	2.06	0.115	98.2	2.1
	22.39	0.176		
TnI·TnC, pH 7.5 (Mg^{2+})	2.35	0.114	66.0	3.4
	24.12	0.171		
TnI·TnC, pH 7.5 (Ca^{2+})	1.57	0.063	79.8	2.0
	26.24	0.225		

[a] TnC was singly labeled with DNZ and its rotational correlation times (θ_i) and anisotropy at zero time (r_{0i}) were determined under various conditions. The TnC in the last three samples was in the presence of TnI as the binary complex TnI·TnC. The anisotropy decay was resolved into two components, with θ_1 referring to the short correlation times and θ_2 to the long correlation time and the corresponding zero-time anisotropy values being r_{01} and r_{02}. The last two columns give the χ_R^2 values for the best one-component (1) and two-component (2) fits.

(θ_1) less than 2 ns (Table III). The long correlation time (θ_2) is 12.46 ns at the high pH and 19.21 ns at the low pH. These results suggest that TnC forms an aggregate at pH 5.2. The two anisotropy components contribute about equally to the limiting anisotropy at pH 7.5, whereas the short decay component contributes only about 25% at pH 5.2. Figure S2 shows the anisotropy data obtained in the presence of Mg^{2+} and Ca^{2+}. The effects of these cations are very small on both correlation times, but Ca^{2+} binding reduces the contribution of the short component to the total anisotropy. Shown in Figure S3 are the anisotropy decays of TnC-DNZ complexed with TnI, determined in the presence of Mg^{2+} and Ca^{2+}. The long correlation time (Table III) is considerably larger than that of uncomplexed TnC-DNZ, reflecting a larger mass of the binary protein complex.

It is of interest to establish to what extent the correlation times observed for TnC-DNZ at the two pH values are distinct

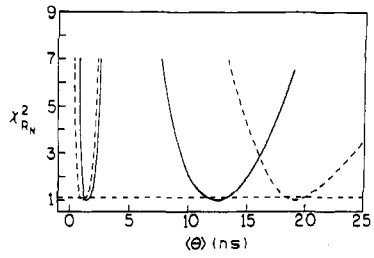

FIGURE 8: Dependence of χ_R^2 on the two correlation times of donor-labeled TnC (TnC-DNZ) at pH 7.5 (—) and pH 5.2 (---). The two curves on the left are the short correlation time (θ_1), and the two curves on the right are the long correlation time (θ_2). One correlation time was held constant, and the other parameters (one θ and two r_i) were varied to minimize χ_R^2. The dashed line indicates the largest value of χ_R^2 with random noise in 67% of repetitive measurements.

from each other. This is accomplished by comparing the χ_R^2 surfaces for the correlation times as shown in Figure 8. The large overlap of the surfaces for the short correlation times obtained at the two pH values precludes any significant difference between them. However, the surfaces for the long correlation times intersect at a χ_R^2 value about 3-fold larger than the minimum value. This result provides a statistical assurance that the increased long correlation time at pH 5.2 does represent a significant structural alteration.

Discussion

The present work was focused on the conformational distributions of troponin C from rabbit skeletal muscle and the effect of acidic pH on the distributions. We consider (a) in what way structural dynamics may play a role in signal transmission in muscle and (b) the extent to which the overall conformation of TnC in neutral solution may be compatible with a crystal structure obtained at an acidic pH. We and others have recently demonstrated that the distribution of intramolecular distances deduced from FRET measurements by frequency domain (Lakowicz et al., 1988; Gryczynski et al., 1988) and time domain (Hass et al., 1988) fluorometry can be very useful for investigations of protein dynamics and perturbation of the dynamics. If the structure is unique and rigid, then a unique single value can be assigned to the D–A distance, as has been found for a protein in the α-helical state (Lakowicz et al., 1990a). The existence of a range of D–A distances indicates that the protein can adopt a variety of conformational states. Diffusion between the donor- and acceptor-labeled sites can alter the apparent distribution (Lakowicz et al., 1990a, 1991b), and recently Lakowicz et al. (1990b) have been able to recover the donor-to-acceptor diffusion coefficient from the frequency domain data. Additionally, an apparent distance distribution could result from a distribution of donor and/or acceptor orientations, due to the dependence of the transfer rate on the orientation factor (Dale et al., 1979). The distribution of D–A distances recovered for TnC in EGTA and at pH 7.5 has a considerable width. While it is not yet possible to quantitatively assess the various factors that can contribute to an observed distribution width, we (Lakowicz et al., 1988) have recently given a qualitative discussion of this problem by estimating possible contributions from fluorophore mobility and uncertainties in the orientation factor. The contribution from the latter is unlikely large because of the presence of mixed polarizations in the energy donor (Haas et al., 1978). On the basis of those considerations, we conclude that the width of 13.3 Å observed at pH 7.5 does reflect the existence of a range of TnC conformers, each of which has a different D–A distance between the same pair of residues. These conformers likely result from global structural changes and/or fluctuations, and the observed distribution width is too large to be explained by a single unique structure of TnC, particularly within the region of the molecule between Cys 98 located at the C-terminal end of the central D/E helix and Met 25 in helix A of the N domain. The data, however, do not readily distinguish between structural fluctuations occurring mainly in the N domain or in the D/E helical linker and therefore cannot establish whether the D/E linker has an appreciable segmental flexibility. This is an important point because potential segmental motions can occur around Gly 89 (corresponding to Gly 92 in chicken TnC) in the central helix. Such motions, if slow compared to the donor decay time, can result in a range of D–A distances and a distribution of the distances. In contrast, diffusive motions that are rapid compared to the decay time can result in narrowing of the apparent distance distribution (Lakowicz et al., 1991b).

The mean distance $\bar{r}$ of the recovered D–A distance distribution at pH 7.5 is appreciably shorter than the previous value determined by conventional FRET methods (Wang & Cheung, 1985). The reason for the discrepancy is unclear. In this connection, we should mention two recent studies that reported distributions of D–A distances for troponin I (Lakowicz et al., 1988) and myosin subfragment 1 (Cheung et al., 1991) with mean distances that were within 2–3 Å of the distances determined by standard FRET methods. It should be noted that $\bar{r}$ is obtained by a procedure in which each conformer is properly weighted. This weighting is not possible when the D–A distance is calculated from average quantum yield or lifetime as is the case with standard FRET methods.

In the presence of Mg^{2+}, sites III and IV located in the C domain are saturated by the cation but sites I and II in the N domain are vacant. Under this condition, $\bar{r}$ at pH 7.5 is significantly reduced with a small apparent effect on the distribution width when compared with apo-TnC. The decreased $\bar{r}$ is in general agreement with previous results obtained from standard FRET measurements (Wang & Cheung, 1986) although the magnitude of the observed decrease is larger in the present work. In the presence of sufficient Ca^{2+}, all four sites are saturated by the cation. It is not entirely clear to what extent Mg^{2+} and Ca^{2+} may elicit similar or identical structural changes upon binding to the same sites III and IV. If the assumption is made that similar structural changes are induced by both cations binding to the same sites, then the binding of Ca^{2+} to the Ca^{2+}-specific sites I and II must result in a significant increase in the mean distance such that the increase is off-set by the decrease induced by saturation of sites III and IV. These compensatory changes may be responsible for the apparently identical mean D–A distances for apo-TnC and TnC fully saturated with Ca^{2+}. Thus, a change of the ionic condition from Mg^{2+} to Ca^{2+} results in a decrease of the hw by 4 Å and an increase of $\bar{r}$ by 7 Å. Similar changes in the distribution parameters are also observed when TnC is complexed to TnI.

It is generally accepted that TnC in relaxed muscle is most likely saturated with Mg^{2+} at sites III and IV, with sites I and II vacant. Upon activation, Ca^{2+} binds to sites I and II and exchanges with bound Mg^{2+}. The exchange is likely because the affinity of sites III and IV for Ca^{2+} is 3–4 orders of magnitude higher than for Mg^{2+}. The present results provide a simple model to relate structural perturbations to calcium activation. We first consider simple explanations for the observed increase in $\bar{r}$ and decrease in hw when Mg^{2+} is replaced by Ca^{2+}. The rate of energy transfer is expected to decrease with decreasing fluctuation dynamics of the labeled polypeptide

segment (Haas et al., 1978b; Lakowicz et al., 1991b). Decreased fluctuation dynamics thus favors longer distances and is expected to shift the distance distribution toward longer distances with an increase in $\bar{r}$. As already mentioned, several factors can also contribute to the apparent distribution width. The short rotational correlation time of TnC-DNZ derived from anisotropy data may reflect a restricted motion of the attached probe or a localized segmental motion of the protein. This motion is more restricted in the presence of Ca^{2+} than in Mg^2. The conclusion is reached on the basis of the model-independent order parameter (Lipari & Szabo, 1982) calculated from anisotropy data: $S^2 = r_{02}/(r_{01} + r_{02})$. A value of $S^2 < 1$ suggests motion with respect to the protein. S^2 is 0.498 in Mg^{2+} and 0.659 in Ca^{2+}. The order parameter can be related to a hypothetical cone semiangle over which the transition dipole of the probe can traverse. The semiangle is 38° in Mg^{2+} and 30° in Ca^{2+}, indicating that the amplitude of the motion is smaller when all four sites are saturated with Ca^{2+} than when only two of the sites are occupied by Mg^{2+}. Wang et al. (1988) recently reported similar changes in the cone semiangle traversed by IAEDANS attached to Cys 98 resulting from replacement of Mg^{2+} by Ca^{2+}. Although we have no anisotropy data for the acceptor eosin attached to Cys 98, it seems reasonable to assume that the motion of the acceptor site also has a smaller amplitude in Ca^{2+} than in Mg^{2+}. Assuming the effective length of the donor to be 15 Å, a decrease of the semiangle by 8° corresponds to a decrease of 1.7 Å in the angular excursion of the probe transition dipole. This decreased angular excursion coupled with a 25% increase in its rotational correlation time indicates a decrease in the restricted mobility. This decrease would lead to an increase rather than decrease in the apparent width. To what extent donor-to-acceptor diffusion occurs in TnC is unknown, but enhanced diffusion in Ca^{2+}-saturated TnC would reduce the apparent width. The width could also be reduced with a concomitant increase in the mean distance if the range of conformations is reduced as recently demonstrated for the transition of mellitin from the random-coil state to an α-helical conformation (Lakowicz et al., 1990a).

The increase in $\bar{r}$ also could be explained by assuming extensive rearrangement of the helices in the N domain as Ca^{2+} binds to sites I and II such that the overall D–A separation was increased. Simulation studies (Herzberg et al., 1986) have shown that Ca^{2+} binding to the low-affinity sites I and II likely induces rearrangements of helices B and C. A consequence of these rearrangements is an altered angular relationship between the N and C domain, which could result in a narrowing of $P(r)$. Since these structural changes are preserved in the TnI·TnC complex, we suggest that altered conformational dynamics may be an important structural feature involved in the transmission of the initial Ca^{2+} signal from sites I and II to distant points along the thin filament.

The interaction between TnI and TnC involves at least two regions of each protein (Sykes et al., 1976; Grabarek et al., 1981). Early studies showed that synthetic oligopeptides corresponding to the segment of TnI residues 104–115 (inhibitory peptides) interacted with TnC (Cachia et al., 1983) and tropomyosin–actin (Talbot & Hodges, 1981), and proton NMR studies suggested that both actin and TnC perturbed some of the resonances of TnI within the stretch of residues 96–116. Recent studies (Leszyk et al., 1987) showed that the region of Cys 98 of TnC is in close contact with the inhibitory region of TnI. Van Eyk and Hodges (1988) examined the contribution of each amino acid residue of TnI sequence 104–115 toward the interactions with TnC and tropomyosin–actin by using a series of inhibitory peptides. These workers showed that the peptides could bind to either TnC or tropomyosin–actin in the presence of Mg^{2+} and suggested that, in the presence of Mg^{2+}, the inhibitory region of TnI in the tropomyosin–troponin complex is favored to interact with tropomyosin–actin, rather than with TnC. When the Ca^{2+}-specific sites are filled, the TnI–(tropomyosin–actin) interaction is suppressed and the TnI–TnC interaction becomes enhanced. Thus, tropomyosin–actin and TnC compete for the same inhibitory region of TnI, and Ca^{2+} binding to TnC switches TnI from a strong interaction with tropomyosin–actin to a strong interaction with TnC. These two strong interactions occur alternately during cycles of excitation–relaxation and may be governed by Ca^{2+}-dependent cyclic changes of conformational flexibility in both proteins. We (Lakowicz et al., 1988) have shown that the mean D–A distance between Trp 158 and Cys 133 in TnI complexed with TnC is little affected by either Mg^{2+} or Ca^{2+} binding to TnC but the half-width of the distribution of the distances is decreased by 10 Å when Mg^{2+} at sites III and IV is displaced by Ca^{2+} and sites I and II are concomitantly saturated with Ca^{2+}. The decreased hw could be due to enhanced site-to-site diffusion and/or increased conformational fluctuations of TnI within the TnI·TnC complex. These initial results suggest that in relaxed muscle the interaction of the inhibitory region of TnI with tropomyosin–actin is favored because the TnI segment is relatively static, allowing optimal contact between the interaction sites. This interaction would in effect prevent strong interaction between the same TnI region and TnC. Upon Ca^{2+} activation the TnI–(tropomyosin–actin) interaction is weakened possibly because of enhanced intramolecular diffusion and/or enhanced conformational dynamics in TnI. The disruption of this interaction allows optimal interaction of the same TnI region with TnC, and this enhanced interaction may be facilitated by enhanced conformational dynamics that occur in the two proteins. While we interpret the Ca^{2+}-modulated strong interaction between TnI and TnC in terms of altered protein dynamics, the difference in affinity between the weak and strong interactions is a factor of 100 (Wang & Cheung, 1985), corresponding to a free energy coupling of -2.8 kcal mol^{-1}. On the basis of binding energetics, Cheung et al. (1987) have proposed that the TnI–TnC linkage is a major Ca^{2+} signal transmitter. The structural basis of the stabilization of this linkage by Ca^{2+} binding to its specific sites may be related to changes in conformational fluctuations in both proteins as well as a more extended or less compact conformation of TnC.

The alteration of the distance distribution observed by lowering the pH from 7.5 to 5.2 is striking. The 9-Å increase in the mean distance can be explained by an elongated molecular shape. This conformation in acidic pH could result from (a) elimination of the putative segmental flexibility or (b) extensive rearrangement of the helices located in the N domain such that helix A in general, and the donor fluorophore in particular, became further away from Cys 98. The acid-induced increase in $\bar{r}$ is consistent with pH-dependent results previously obtained by standard energy transfer measurements (Cheung & Wang, 1985; Wang et al., 1989) and the FRET distance between Tb^{3+} bound to sites I and II in the N domain and a probe attached to Cys 98 (Wang et al., 1987). The present results additionally show that the increased distance observed at pH 5.2 is accompanied by a change in dynamic fluctuations that are responsible for the wide distribution observed at neutral pH. The narrowing of the distribution could result partly from increased probe mobility. However, the short correlation time is only 25% shorter at pH 5.2. The

Table IV: Rotational Correlation Times of Monomeric TnC Computed for a Prolate Ellipsoid of Revolution[a]

	$h = 0$			$h = 0.2$			$h = 0.3$			$h = 0.4$		
γ	θ_a (ns)	θ_b (ns)	θ_h (ns)	θ_a (ns)	θ_b (ns)	θ_h (ns)	θ_a (ns)	θ_b (ns)	θ_h (ns)	θ_a (ns)	θ_b (ns)	θ_h (ns)
2	7.9	5.5	6.9	10.1	7.1	8.9	11.3	7.8	9.8	12.3	8.6	10.8
3	12.3	5.9	9.0	25.8	7.6	11.6	17.5	8.5	12.9	19.2	9.3	14.2
5	24.4	6.5	12.7	31.2	8.3	16.3	34.6	9.1	17.9	38.0	10.0	19.7
8	49.1	6.7	15.8	62.8	8.6	20.3	69.6	9.5	22.4	76.4	10.5	24.7
10	71.2	6.8	17.1	91.1	8.7	21.9	100.9	9.7	24.4	110.8	10.6	26.7

[a] Rotational correlation times θ_a and θ_b were computed with a measured partial specific volume of 0.719 mL g^{-1} at 20 °C for different hydration values (h) expressed in grams of H_2O per gram of protein. θ_h is the harmonic mean of θ_a and θ_b. γ (axial ratio) is the ratio of the long (a) to the short (b) semiaxes.

decrease may not be sufficient to cause a substantial change in the hw. If the conformations of TnC at pH 5.2 are severely constrained, the apparent width could be reduced to the range 1–3 Å, as has been demonstrated with mellitin (Lakowicz et al., 1990a). If we assume that in the pH 5.2 conformation donor and acceptor mobility persists and this mobility contributes to the observed distribution width, then the 7-Å half-width would be very close to that expected of a highly constrained structure with little or no large-scale conformational fluctuations. Thus, the conformation of the protein at pH 7.5 is not unique and the protein does not appear to have an overall extended conformation as the crystal structure predicts. However, the protein is more elongated at pH 5.2 and this elongated structure is unlikely to undergo extensive conformational fluctuations.

The anisotropy decay of TnC singly labeled at Met 25 with DNZ shows two components under all conditions studied. These results are comparable to those recently reported by Wang et al. (1988) for TnC labeled with IAEDANS at Cys 98 determined by time domain measurements. If TnC is approximated by a prolate ellipsoid of revolution, the two expected rotational correlation times θ_a and θ_b can be readily calculated from the Perrin equation with use of appropriate frictional coefficients (Koeing, 1975) for various axial ratios. These calculation are shown in Table IV for different assumed values of hydration (h). Regardless of the value of h, the computed short correlation times (θ_b) are considerably larger than the observed short correlation times (θ_1). These results rule out the possibility that θ_1 may correspond to the rotation of the short axis (θ_b) and strongly suggests that θ_1 more likely reflects localized motions of the attached fluorophore and θ_2 reflects the overall motions of the protein. This conclusion is supported by the results that, in TnI·TnC, θ_1 is hardly affected, whereas θ_2 is considerably lengthened, reflecting the increased molecular mass of the protein complex. The observed long correlation time (θ_2) can be compared with the harmonic mean (θ_h) of θ_a and θ_b. It is seen that θ_2 is comparable to θ_h for an axial ratio of 2–3 and a hydration ≥ 0.4. A hydration value of 0.4–0.5 probably is a realistic estimate for TnC (Hubbard et al., 1988), and an axial ratio of 2–3 for TnC is unlikely to be in gross error.

At pH 5.2, θ_1 is small and cannot be statistically distinguished from that observed at pH 7.5. However, the increased value of θ_2 at the lower pH is distinct from that obtained at pH 7.5. This result could be simply explained by a more elongated structure in which the axial ratio was increased by a factor of 2. This increase would be consistent with the observed increase in $\bar{r}$. However, skeletal TnC has recently been shown to self-associate with decreasing pH from 7.5 to 5.2, and at pH 5.2 the protein is a dimer (Wang et al., 1989). The larger θ_2 (19.21 ns) value reflects the motion of a dimeric structure that exists at pH 5.2. The computed rotational correlation times for dimeric TnC are given in Table S2. These calculations indicate that the dimer is unlikely to have an end-to-end linear structure. Both θ_a (76 ns) and θ_h (39 ns) are much larger than θ_2 for an axial ratio of about 5 and $h = 0.4$. If h remains about 0.4 or somewhat less at the acidic pH, the dimer may have an axial ratio that is either comparable to or less than that for the monomer at pH 7.5. The present data are not sufficient to establish whether the dimer has a side-by-side structure or a short linear structure in which the two monomers overlap each other. A dimeric structure can easily impose a constraint on large-scale protein dynamics and result in a narrower distribution of intramolecular distances. We believe that the narrower distribution at pH 5.2 is a consequence of dimer formation. This finding is consistent with our view that TnC monomers in neutral solution undergo dynamic fluctuations and unlikely have an extended conformation in comparison with the pH 5.2 conformation.

Recent X-ray scattering data collected from neutral solutions of TnC appeared to be best fitted to a model in which the central helix is bent (Heidorn & Trewhella, 1988). The C and N domains are rotated with respect to each other such that they are closer to each other than in the crystal. The centers of mass of the two globular domains are closer by about 5 Å, and the distance of closest approach for the ellipsoid surfaces used to approximate the domains is smaller by 9 Å. These results are compatible with our observation of a decrease in $\bar{r}$ when the pH is changed from 5.2 to 7.5. It should be noted that a similar X-ray scattering study of TnC (Hubbard et al., 1988) reported scattering profiles that were similar to those obtained by Heidorn and Trewhella (1988) but concluded that the average conformation of the protein at pH 6.8 was consistent with the crystal structure.

In summary, the method of FRET was used to determine the distribution of intramolecular distances in skeletal TnC and obtain information bearing on the dynamic nature of the protein. The solution conformation of individual TnC molecules is less elongated at pH 7.5 than at pH 5.2. The more elongated structure that prevails at acidic pH is compatible with a dimeric structure. A flexible central helix may be an important structural feature that allows alteration of protein dynamics. The results also suggest that Ca^{2+} activation in muscle may be accompanied by altered protein dynamics in TnC and that this change may be necessary for the stabilization of the TnI–TnC linkage and play a role in the transmission of Ca^{2+} signal in muscular contraction.

Supplementary Material Available

Three figures showing the emission spectra of donor-labeled and donor–acceptor-labeled TnC and the frequency domain anisotropy data of donor-labeled TnC determined in the presence of Mg^{2+} and Ca^{2+} and complexed with TnI, and two tables showing the detailed multiexponential analysis of the donor decays of TnC–DNZ and TnC–DNZ–IAE and the computed rotational correlation times of dimeric TnC (6 pages). Ordering information is given on any current masthead page.

Registry No. Ca, 7440-70-2; Mg, 7439-95-4.

REFERENCES

Amir, D., & Haas, E. (1987) *Biochemistry 26*, 2162–2175.

Bevington, P. R. (1969) *Data Reduction and Error Analysis for the Physical Sciences*, McGraw-Hill, New York.

Cachia, P. J., Sykes, B. D., & Hodges, R. S. (1983) *Biochemistry 22*, 4145–4152.

Cheung, H. C., & Wang, C.-K. (1985) *Biochemistry 24*, 3364.

Cheung, H. C., Wang, C.-K., & Garland, F. (1982) *Biochemistry 21*, 5135–5142.

Cheung, H. C., Wang, C.-K., & Malik, N. A. (1987) *Biochemistry 26*, 5904–5907.

Cheung, H. C., Gryczynski, I., Malak, H., Wiczk, W., Johnson, M. L., & Lakowicz, J. R. (1991) *Biophys. Chem.* (in press).

Dale, R. E., Eisinger, J., & Blumberg, W. E. (1979) *Biophys. J. 26*, 161–184.

Forster, Th. (1948) *Ann. Phys. (Leipzig) 2*, 55–75 (translated by R. S. Knox, University of Rochester).

Grabarek, E., Drabikowski, W., Leavis, P. C., Rosenfeld, S. S., & Gergely, J. (1981) *J. Biol. Chem. 256*, 13121–13127.

Gratton, E., Lakowicz, J. R., Maliwal, B., Cherek, H., Laczko, G., & Linkeman, M. (1984) *Biophys. J. 46*, 479–486.

Haas, E., Wilchek, M., Katchalski-Katzir, E., & Steinberg, I. Z. (1975) *Proc. Natl. Acad. Sci. U.S.A 72*, 1807–1811.

Haas, E., Katchalski-Katzir, E., & Steinberg, I. Z. (1978) *Biochemistry 17*, 5064–5070.

Haas, E., McWherter, C. A., & Scheraga, H. A. (1988) *Biopolymers 27*, 1–21.

Heidorn, D. B., & Trewhella, J. (1988) *Biochemistry 27*, 909–915.

Herzberg, O., & James, M. N. G. (1985) *Nature 313*, 653–659.

Herzberg, O., Moult, J., & James, M. N. G. (1986) *J. Biol. Chem. 261*, 2638–2644.

Hubbard, S. R., Hodgson, K. D., & Doniach, S. (1988) *J. Biol. Chem. 263*, 4151–4158.

Johnson, M. L. (1983) *Biophys. J. 44*, 101–106.

Koeing, S. (1975) *Biopolymers 14*, 2421–2423.

Lakowicz, J. R., & Maliwal, B. P. (1985) *Biophys. Chem. 21*, 61–78.

Lakowicz, J. R., Laczko, G., Cherek, H., Gratton, E., & Limkeman, M. (1984) *Biophys. J. 46*, 463–477.

Lakowicz, J. R., Cherek, H., Maliwal, B. P., & Gratton, E. (1985) *Biochemistry 24*, 376–383.

Lakowicz, J. R., Laczko, G., & Gryczynski, I. (1986) *Rev. Sci. Instrum 57*, 2499–2506.

Lakowicz, J. R., Johnson, M. L., Wiczk, W., Bhat, A., & Steiner, R. F. (1987) *Chem. Phys. Lett. 138*, 587–593.

Lakowicz, J. R., Gryczynski, I., Cheung, H. C., Wang, C.-K., Johnson, M. L., & Joshi, N. (1988) *Biochemistry 27*, 9149–9160.

Lakowicz, J. R., Gryczynski, I., Wiczk, W., Laczko, G., Prendergast, F. G., & Johnson, M. L. (1990a) *Biophys. Chem. 36*, 99–115.

Lakowicz, J. R., Kubsa, J., Wiczk, W., Gryczynski, I., & Johnson, M. L. (1990b) *Chem. Phys. Lett. 173*, 319–326.

Lakowicz, J. R., Gryczynski, I., Wiczk, W., Kusba, J., & Johnson, M. L. (1991a) *Anal. Biochem.* (in press).

Lakowicz, J. R., Wiczk, W., Gryczynski, I., Szmacinski, H., & Johnson, M. L. (1991b) *Biophys. Chem. 39*, 79–84.

Leszyk, J., Collins, J. H., Leavis, P. C., & Tao, T. (1987) *Biochemistry 26*, 7042–7047.

Lipari, G., & Szabo, A. (1982) *J. Am. Chem. Soc. 104*, 4559–4563.

Maliwal, B. P. & Lakowicz, J. R. (1986) *Biochim. Biophys. Acta 873*, 161–172.

McCubbin, W. D., Oikawa, K., Sykes, B. D., & Kay, C. M. (1982) *Biochemistry 21*, 5948–5956.

Perry, S. V., & Cole, H. A. (1974) *Biochem. J. 141*, 733–743.

Satyshur, K. A., Rao, S. T., Pyzalska, D., Drendel, W., Greaser, M., & Sundaralingam, M. (1988) *J. Biol. Chem. 263*, 1628–1647.

Sundaralingam, M., Bergstrom, R., Strasburg, G., Rao, S. T., Roychowdhury, P., Greaser, M., & Wang, B. C. (1985a) *Science 227*, 945–948.

Sundaralingam, M., Drendel, W., & Greaser, M. (1985b) *Proc. Natl. Acad. Sci. U.S.A. 82*, 7944–7947.

Syska, H., Wilkinson, J. M., Grand, R. J. A., & Perry, S. V. (1976) *Biochem. J. 153*, 357–387.

Talbot, J., & Hodges, R. S. (1981) *J. Biol. Chem. 256*, 2798–2802.

Van Eyk, J. E., & Hodges, R. S. (1988) *J. Biol. Chem. 263*, 1726–1732.

Wang, C.-K., & Cheung, H. C. (1985) *Biophys. J. 48*, 727–739.

Wang, C.-K., & Cheung, H. C. (1986) *J. Mol. Biol. 191*, 509–521.

Wang, C.-L. A., Zhan, Q., Tao, T., & Gergely, J. (1987) *J. Biol. Chem. 262*, 9636–9640.

Wang, C.-K., Liao, R., & Cheung, H. C. (1988) *Proc. SPIE (Int. Soc. Opt. Eng.) 900*, 139–146.

Wang, C.-K., Lebowitz, J., & Cheung, H. C. (1989) *Proteins: Struct., Funct., Genet. 6*, 424–430.

Wilkinson, J. M. (1974) *Biochim. Biophys. Acta 359*, 379–388.